Journal of Geoscience and Environment Protection, 2025, 13(12), 326-352
https://www.scirp.org/journal/gep
ISSN Online: 2327-4344
ISSN Print: 2327-4336

Groundwater Potential Estimation and Aquifers Vulnerability in the Tongo-Bassa Watershed (Douala Sedimentary Basin, Cameroon)

Naëlle Kelly Gamene[1], Adoua Njueya Kopa[1*], Flavie Laura Zangmene[2], Paulin Sainclair Kouassy Kaledje[1], Rodrigue Tetang Kouo[1], Rodrigue Talla Toteu[1], David Guimolaire Nkouathio[1], Lucas Kengni[1]

[1]Faculty of Science, University of Dschang, Dschang, Cameroon
[2]Faculty of Science, University of Douala, Douala, Cameroon
Email: *njuedou@yahoo.fr

How to cite this paper: Gamene, N. K., Njueya Kopa, A., Zangmene, F. L., Kouassy Kaledje, P. S., Tetang Kouo, R., Talla Toteu, R., Nkouathio, D. G., & Kengni, L. (2025). Groundwater Potential Estimation and Aquifers Vulnerability in the Tongo-Bassa Watershed (Douala Sedimentary Basin, Cameroon). *Journal of Geoscience and Environment Protection, 13,* 326-352.
https://doi.org/10.4236/gep.2025.1312017

Received: August 27, 2025
Accepted: December 8, 2025
Published: December 11, 2025

Abstract

The present study was carried out in Douala megacity of Cameroon to highlight suitable aquifer that could be exploited by population or municipality authorities, to promote access to safe potable water and avoid or reduce water borne deseases. Specifically, this study aimed to assess structure of Quaternary-Mio-Pliocene aquifer and its potentiality and vulnerability distribution, within Tongo-Bassa watershed through piezometry and geoelectrical survey. Then, 29 wells were assessed by piezometric study both in wet and rainy season, while thirty-two (32) vertical electrical sounding were performed through geohydraulic parameters (Permeability, Porosity, Transmissivity, Longitudinal Conductance and Hydraulic resistance). Piezometric survey in shallow aquifer globally show a convergent flow (from South East to North West direction) to defined outlet and this masks heterogeneities of flowing from wet to dry season. Vertical electrical soundings inversion revealed 10 (HK, KH, HA, HKH, H, K, AK, QH, KQ, HKQ) curves types which confirm lithological heterogeneities. Borehole lithologs correlated to geoelectric section allow distinguishes unconfined and semi-confined/confined aquifers exploited by population. Unconfined aquifer with depth less than 28 m, fairly adapted for local level with limited consumption for private water supply ($0.02 < Tr < 14.67$ m^2/day) show that 87.87% of the area are more vulnerable ($-0.58 < \text{Log } C < 0.96$). Semi-confined/confined aquifers with depth less than 70 m, with good groundwater potential ($0.50 < Tr < 42.05$ m^2/day) adapted for groundwater supply that municipality authorities can exploit to manage groundwater development in Douala Sedimentary Basin, show that only 39.39% of the area are vulnerable ($0.29 < \text{Log } C < 0.95$).

Keywords

Groundwater Management, Piezometry, Vertical Electrical Sounding, Geohydraulic Parameters, Aquifer Vulnerability Index

1. Introduction

Socio-economic development of any society inevitably requires an access to safe and good water resource. Water is a vital resource by excellence, fuelling economic growth and contributing to the health of ecosystems (Akakuru et al., 2023; Ibuot et al., 2022; Njueya et al., 2012; Obiora & Ibuot, 2020). Around 2 billion people in the world do not have access to safe drinking water, while 3.6 billion are deprived of sanitation services. These deficiencies are exacerbated by population growth, greater rainfall fluctuations and pollution, making the water issue a major threat to economic progress, poverty eradication and sustainable development. Due to fast population growth, this access to safe and potable water becomes difficult in more developing country as in Cameroon, where water demands remain high and surface water are polluted by anthropogenic activities (Ngo Billong et al., 2023; Njueya et al., 2012; Nlend et al., 2021). In Douala Sedimentary Basin, despite the abundance of surface water and intense rainfall (about 4000 mm/year), groundwaters are the main resources use by population to satisfy their waters need (Ketchemen Tandia et al., 2017; Ngo Billong et al., 2023; Njueya et al., 2012; Nlend et al., 2021). However, this resource is subject to various forms of pollution depending on the type of sanitary installations and anthropogenic activities like industrial and domestic discharges, as suggested by many authors (Bentekhici et al., 2018; Emvoutou et al., 2018; Fantong et al., 2016; Ketchemen Tandia et al., 2017; Ngo Billong et al., 2023; Ngo Boum et al., 2015). The main factors of pollution are the lack of environmental sanitation and the precarious hygiene conditions of populations (Hounsounou et al., 2016). Douala V municipality, traversed by the Tongo-Bassa watershed, embodies various urban and peri-urban aspects, resembling a miniature Douala with most of the city's vulnerable neighborhoods prone to flooding risks. According to Nsegbe (2021), Makepe-Missoke for example, serves as a living and working space but primarily as a dumping ground for various waste from not only the neighborhood but also the rest of the city. In the study area during rainy season, there is recurrence of flooding due to the saturation of shallow aquifer; and many functional wells and boreholes are abandoned, due to contamination of water, while others wells and boreholes show good water quality. A study made by Nsegbe (2021) shows that the poor physicochemical quality of Makepe-Missoke waters is due to the high abundance of faecal pollution bioindicator bacteria, causing not only waterborne bacterial diseases but also parasitic gastrointestinal diseases and cutaneous mycoses. The issue of water resource quality is closely linked to the choice of good aquifer to be exploited and the protection of groundwater. Given the accessibility and cost challenges of decontami-

nation techniques, preventive measures become crucial. According to El Kayssi et al. (2020), Igboama et al. (2021) and Oluchi et al. (2024), the fact that the quality and quantity of groundwater are at high risk, particularly threatened directly by human activities such as overexploitation, agriculture, population growth, urbanization, wastewater leakage, and indirectly, through climate change, seawater intrusion, and global warming it is important to making smarter use of the groundwater potential resources by mapping where the potential are high and less vulnerable. This, preventive mapping of aquifers potential and vulnerability could help develop right policy to well manage groundwater in a given area. Several methods (directs and indirects) for assessing groundwater potential have been developed around the world. The fact that direct methods as pumping tests for example for assessing groundwater potential are expensive, time-consuming and sometimes difficult to interpret, indirect methods as geoelectrical surveys have been developed to save time and money, when evaluate this groundwater potential through determination of geohydraulic parameters (Akakuru et al., 2023; Ibuot et al., 2024, 2022, 2019; Sinaga et al., 2023), and aquifer vulnerability (Ibuot et al., 2022, 2017; Obiora et al., 2015; Oli et al., 2020; Obiora & Ibuot, 2020) in sedimentary area as well as basement area. Geoelectrical survey through analysis of apparent resistivity field data have proved to be useful as indirect methods in groundwater study to analyse aquifer geometry, aquifer geohydraulic properties, groundwater quality and vulnerable areas. In fact, according to many authors (Ibuot et al., 2024; Oli et al., 2020; Oluchi et al., 2024), groundwater flow, availability, quality and potential are controlled by aquifer properties such as porosity, permeability, resistivity, layer thickness and aquifer yield. The applications of this indirect and non-invasive techniques have the potential to predict spatially and more efficiency the distributions of the aquifer geohydraulic parameters. Despite the fact that many studies have demonstrated the effectiveness of geo-electrical survey for prediction and efficient management of aquifers by determining the potential and vulnerability of exploitable zones for water supply, no such study has yet been carried out in the Douala sedimentary basin. In fact, such a study could be useful for the population and municipal authorities in charge of the city, both from a technical and financial point of view, as an alternative to conventional hydrogeological studies, which are very costly due to the drilling boreholes and pumping tests involved. Then, this study carried out during year 2021 to 2022, aimed to assess and mapping for the first time, the potential and vulnerability distribution of the Tongo-Bassa aquifer using combination of piezometric survey and electrical resistivity data.

2. Overview of the Study Area

2.1. Location, Climatology and Hydrography

This study focuses on the Tongo-Bassa watershed, one of the sub-basin of the Douala Sedimentary Basin (DSB), located on the left bank of the Wouri River. Located between coordinates 4˚01'38" to 4˚05'55" North and 9˚43'03" to 9˚47'50"

East, the Tongo-Bassa watershed belongs to the district of Douala V (Figure 1). The Douala V sub-division, is a very active cosmopolitan city covering an area of 210 km^2, with a population of around 1,000,000 and a population density of 4095 inhabitants per km^2. The density of its population stems from the fact that the majority of the city of Douala's infrastructure is found in this sub-division despite the fact that it is not very industrialised (2.5% of Douala's industrial establishments; Amaneudjeu, 2019).

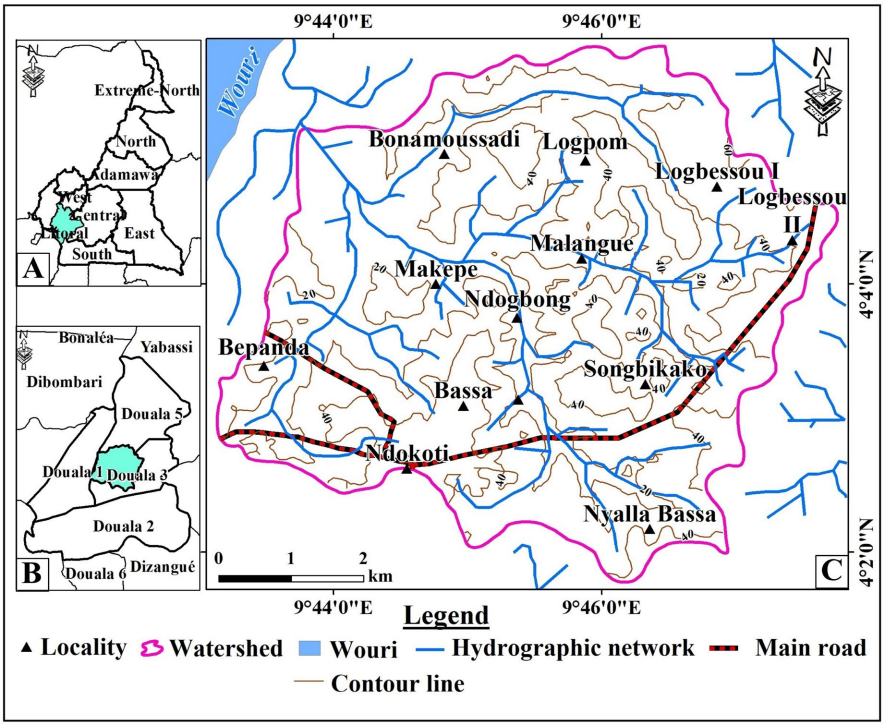

Figure 1. Location of the study area (A): the Littoral Region of Cameroon; (B) the Tongo-Bassa catchment area in the Littoral Region; (C) map of the Tongo-Bassa catchment area and topographical background of Douala V.

The dynamics of land use show progressive urbanisation invading the small villages, which have gradually been integrated into the modern city. Many authors (Ketchemen Tandia et al., 2017; Nlend et al., 2021; Ngo Boum et al., 2015; Takem et al., 2015) reveals the equatorial nature of the climate which would be influenced by the proximity of the area to the Mount Cameroon and downward trend in rainfall with an average of 4000 mm/year, and average annual temperature of 27˚C, considering data from 1951 to 2016 recorded by Douala meteorological station (Nlend et al., 2021). The area has two mains seasons, a long rainy season from March to November and short dry season from December to February. The maximum daily amount of rainfall are recorded in July and August (742.4 mm), while the minimum daily amount are recorded in December and January (34 mm). The DSB has hydrographic network including numerous creeks, mangrove swamps and marshy areas. The urban area is drained by the

Tongo-Bassa, Mbopi, Bobongo, Mbanya, Bounadouma and Mgoua rivers, which join the Wouri and Dibamba. The Tongo-Bassa (**Figure 1(c)**) is the largest catchment in the economic city, with a drainage area of almost 40 km^2. These 10 km-long catchments have many tributaries, including the Ngongue, Kondi, petit Tongo-Bassa and Moussadi. It flows through several districts, such as Makepe-Missoke, where it becomes a tributary known as the Ngongue, the main watercourse in the sub-catchment bearing that name. The hydrographic network in this dense basin, which is supercharged by numerous drains, is of the subdendritic to subparallel type.

2.2. Geology and Hydrogeology

Many authors (Feumba, 2015; Ketchemen Tandia, 2011; Mbog et al., 2019) highlights in DSB, the predominance of ferralitic soils, divided into two types: yellow ferralitic soils derived from sandy and sandy-clay sedimentary rocks, and the little-represented red ferralitic soils derived from the granite-gneiss bedrock (Ndjigui et al., 1999). In addition to the ferralitic soils, there are hydromorphic soils that are generally clayey, poorly developed soils and rough mineral soils. The Tongo-Bassa river flows through a vast plain with a very gentle slope at altitudes of no more than 62 m. Slope modelling in the study area identifies two types of landscape: flat (92.88%) with slopes between 0˚ and 4.61˚ and undulating (7.12%) with slopes between 4.61˚ and 8.17˚. The DSB covers an area of 19000 km^2, of which 7000 km^2 is emerged (Mbesse, 2014). It is bounded to the North by the Cameroon Volcanic Line, to the South by the Northern limit of the Kribi-Campos Sub-basin (KCSB), to the west by the Atlantic Ocean and to the east by the Metamorphic Basement rocks of Central African Fold Belt. According to Tamfu and Batupe (1995), the history of origin and structure of DSB are associated with the opening of South Atlantic Ocean during the breakup of Gondwanaland. The lithostratigraphy of DSB is made of sequences laying unconformable to the Precambrian basement and ranging from Cretaceous rocks to recent alluviums in the Wouri estuary (Nguene et al., 1992; Regnoult, 1986). This lithostratigraphy can be divided in three main units in function of geodynamic and sedimentary evolution (Mvondo, 2010; Ngueutchoua, 1996; Regnoult, 1986). From the bottom to the top we have:

- The Late Cretaceous units, with thickness ranging from 400 to 2000 m and consists of three formations. Then we has: 1) Moundeck formation (Aptian Cenomanian) made of continental and fluvio-deltaic deposits (clays, coarse-grained sands, sandstones); 2) Logbadjeck formations (Cenomanian-Campagnian) discordant onto Mundeck formation and made of sand, sandstones, limestones and clays; 3) Logbaba formations (Maastrichian) mainly composed of sandstone, sand, and fossils shales;
- The intermediate units, with thickness varying from 300 to 1000 m and consists of two formations. Firstly, there is Nkappa formation (Paleocene-Eocene), made of calcareous sandstones, marls and clays with lenses of sand and

fine to coarse grained sandstone. Secondly we have Souellaba formation (Oligocene), lying unconformably on Nkappa deposits and made of sandstones, marls deposits with some interstratified lenses, shales, clayed sand and gravelly sand;

- The upper unit, consists of Matanda (Miocene) and Wouri (Pliocene-Pleistocene) formations. Matanda formations are dominated by deltaic interstratified facies with volcano-clastic layers. These volcanic rocks consist of scoria and basalt (Njiké Ngaha, 2004). Wouri formations consists mainly of indurate lateritic layers, gravelly and sandy deposits with a clayey or kaolinic matrix.

In this paper, we focus on this last unit of DSB made of Quaternary/Mio-Pliocene deposits which constitute a regional and multi-layered aquifer mainly exploited by wells and borehole in Douala and known as shallow aquifer (Emvoutou et al., 2018; Ketchemen Tandia et al., 2017; Ngo Boum et al., 2015). This multilayered aquifer has a maximum thickness of 70 m in the SE (East of the Wouri) where the study area belonging, and consists of sands, sandy clays and lenses of clays (Emvoutou et al., 2018; Ngo Boum et al., 2015; Njueya et al., 2012; Takem et al., 2015). According to Ketchemen Tandia (2011), layers with high content of clays has resistivity less than 500 Ω·m, while those rich in sands where aquifers can be found has resistivity greater than 500 Ω·m and the right value to identify good aquifer with soft and potable water should be ranged between 1000 and 2000 Ω·m. In this complex of shallow aquifers two mains levels are distinguishes: unconfined aquifers, with depth less than 20 m (1 to 20 m); and semi confined or confined aquifers, with depth less than 200 m (20 to 200 m). This aquifer is characterized by a high recharge, ranged from 600 to 700 mm/year and low groundwater flows about 5 to 7 m/day (Ketchemen Tandia, 2011; Nlend et al., 2021). Location areas of recharge in Tongo-Bassa watershed correspond to most elevated points (66 and 50 m.a.s.l respectively) as Logbaba, Malangue, Logbessou and Nyalla (Akoachere et al., 2019; Ketchemen Tandia et al., 2017; Nlend et al., 2021). According to Ketchemen Tandia (2011), almost all the boreholes drilled in the DSB tap several aquifers and are not rigorously subjected to pumping tests after completion, which makes it difficult to assess the hydraulic potential of the various aquifers identified. However, several authors estimate that groundwater productivity of these aquifers are variable and show respectively, yields ranged from 1 to 250 m^3/h; Transmissivity from $4.6 * 10^{-4}$ m^2/h to $6.8 * 10^{-2}$ m^2/s; Permeability from $2.6 * 10^{-5}$ to 0.195 m/s and Storage coefficient from $2.4 * 10^{-5}$ to $7.4 * 10^{-5}$ m^{-1} (Emvoutou et al., 2018; Fantong et al., 2016; Ketchemen Tandia, 2011; Njueya et al., 2012). The shallow aquifers in the Tongo Bassa catchment are recharged mainly from rainfall (Ngo Boum et al. 2015), with groundwater flows trending predominantly NE-SW and SE-NW regardless of the season. The associated watercourses ensure constant drainage of the aquifers throughout the year. According to Akoachere et al. (2019), Ketchemen Tandia et al. (2017) and Takem et al. (2015), the direct recharge of unconfined aquifers during rainy season makes them more vulnerable to pollution by waste water from anthropogenic activities

due to poor sanitation conditions. Monitoring of water quality in the study area suggested that Western and South-eastern part of the Tongo-bassa watershed is more polluted and vulnerable than Eastern and Northern part (Akoachere et al., 2019; Ketchemen Tandia et al., 2017; Ngo Boum et al., 2015).

3. Materials and Methods

3.1. Piezometry

Piezometric study was carried out within the quaternary aquifer which correspond to shallow aquifer, in order to assess the groundwater flow pattern during the rainy and dry seasons. To achieve this, field surveys were carried out and the data obtained was processed in the laboratory. Concerning fields campaigns, during the initial field campaigns, the aim was to identify all the access wells that could be subject to piezometric monitoring and to describe them in order to identify only those that exploited the shallow aquifer. At the end of this campaign, of the 85 wells identified, only 29 were selected for piezometric monitoring (Figure 2), as they met this criterion and were fairly widespread and representative of the site.

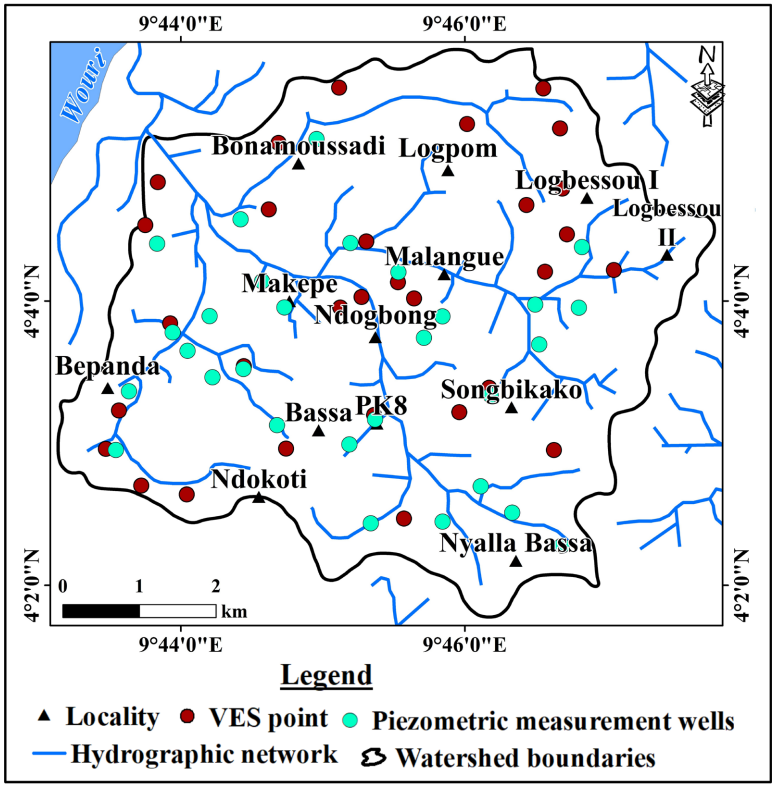

Figure 2. Sample map showing piezometric network and VES points.

For the measurements, a 100 m long piezometric probe with dual signalling (light and sound) was used. After measurements at each point, a GARMIN (etrex-20) GPS was used to record the geographical coordinates.

Static levels were measured over a one-year period (from January to December 2022) with a constant 30-day interval like suggest many authors (Gilli et al., 2008). The data were used to calculate the piezometric level of each water point through the formula (Equation (1)):

$$Np = Z - Ns \quad (1)$$

where Np = Piezometric level, Z = altitudinal elevation of the point, Ns = Static level.

In order to reduce the margin of error when taking the water level and altitude of the points, the reference level for the altitude of a point is that of the surface of the ground. Thus, for a well with a curbstone, the static level and altitude data taken at the curbstone were corrected by subtracting the value of the curbstone from the values of the water level obtained from the probe and the altitude obtained from the GPS. On the other hand, level of altitude was corrected through analysis of SRTM images by Arcgis software and raster image of topographic map of Douala produced by Dumord (1968). Once the calculations had been made, the data were used to produce two iso-piezometric maps of the Tongo-Bassa catchment (one in the dry season and another in rainy season), using kriging methods in Surfer 16 software.

3.2. Electrical Resistivity Survey

For this study, 32 vertical electrical soundings (VES) were carried out at pre-selected stations in the watershed (**Figure 2**), using the WDJD-3 resistivity meter with its accessories (04 coils, 04 electrodes, 02 connectors and 03 hammers). The Schlumberger quadrupole configuration was used for each VES, with half current electrodes (AB/2) separation of 1.5 to 90 m, and half potential electrodes (MN/2) separation of 0.5 to 5 m. According to many authors (Ibuot et al., 2024; Obiora et al., 2016, Obiora & Ibuot 2020) who used this configuration, its well adapted for the field where structure are complex vertically as horizontally like in DSB. In the field, the measurement procedure for a given VES consisted to send a low-intensity current through injection electrodes AB, and measure the potential difference through potential electrodes MN located on either side of central axis point (O). During the various measurement, the depth of investigation was increased by gradually varying the positions of electrodes A and B from AB/2 = 1.5 m to AB/2 = 90 m. Electrodes M and N were kept fixed for a series of measurements. In order to avoid the phenomena associated with energy losses generally known as "breeze blowing", two disengagements are carried out during each sounding. When the clutch is disengaged, the position of M and N is changed from MN/2 = 0.5 m to MN/2 = 5 m. The purpose of disengagement is to increase the distance MN in order to increase the current intensity and obtain better measurement values while eliminating noise. The resistivity metre measured the potential difference generated and converted it to apparent resistivity (ρ_a) which are used to plot a graph manually or by computer software. The manual procedure consisted to plot in a

bi-logarithmic graph, apparent resistivity against half-electrodes spacing and curves obtained were smoothened to remove a noisy signature or the effects of lateral inhomogeneities (Eyankware et al., 2021). Practically, the values of apparent resistivity were imputed into computer software program (Ipi2win) for the computer modelling which generate a set of 1-D curves of vertical electrical sounding (VES) from where the values of true resistivity, thickness and depth of each layer were obtained. It is noticed that, this software applies one-dimensional geophysical inversion using the damped least square method through which the observed data is compared to a synthetic model. The acceptability of the result model is based on the fitness criteria between the observed and calculated apparent resistivity curves. Qualitative interpretation of VES curves and quantitative interpretation of the result (**Figure 3**) was based on field observations of wells and lithological log of boreholes available (case of F1 in the study area). This procedure helps to reduce the ambiguities in the interpretation stage and enhanced the reliability and quality of the modelled results (Ibuot et al., 2024; Obiora et al., 2016).

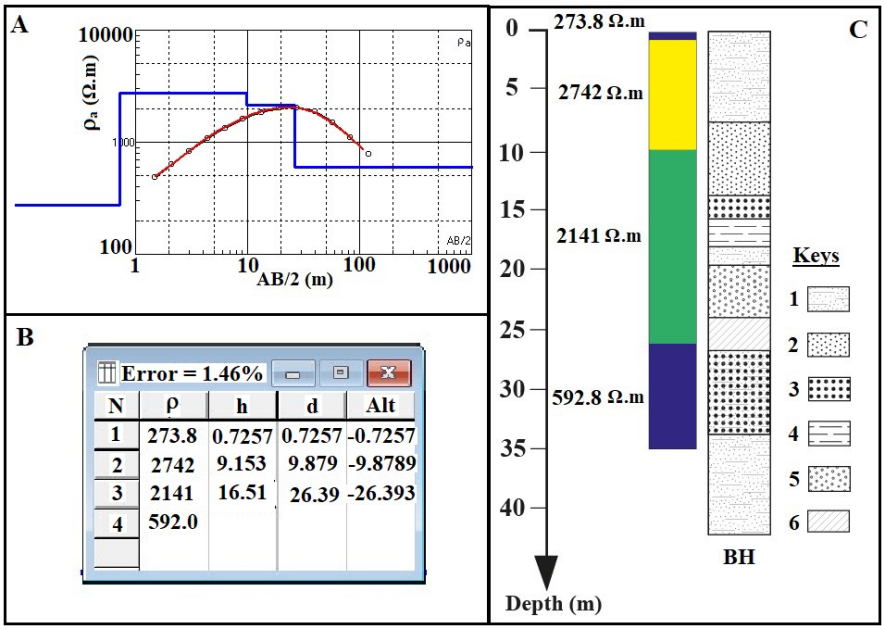

Figure 3. Sample of VES results obtained after modelling correlated with borehole lithology. (A) Curve model; (B) table obtained from modelization showing layers structures with through resistivity and layer thickness; (C) correlation of geo-electrical section with borehole lithology; 1: Sandy clay material; 2: Fine to Medium sand with or no little clay; 3: Coarse grain sand (aquifers); 4: Grey Clayey sand; 5: Medium sand with little or no clay; 6: Mottled clays.

The root means square error (RMSE) less than 3% was used in assessing the extend of fit, and the interpreted curves. Based on auxillary curve matching techniques (Orellana & Mooney, 1966), to deduce the approximate number of layers, three to five layers was assigned to the curve models obtained after a number of iterations made by the software. **Figure 3** shows an example of curve with table

model obtained, geoelectrical section and correlation of the results with borehole lithologs. Based on litho-logs correlation to VES modelled and previous study on DSB area (Emvoutou et al., 2018; Ketchemen Tandia, 2011; Ngo Boum et al., 2015; Njueya et al., 2012), there is multi-layered aquifer, but two main aquifers are distinguish: unconfined aquifer, less than 20 m depth and semi-confined/confined aquifer between 20 - 35 m depth (**Figure 3**). In addition to this observation, it can be seen that in these aquifers, layers rich in sand have the highest resistivities, whereas when clays are abundant, resistivity values drop as well as in the sands aquifers.

Iso-apparent resistivity maps help to provide information on the lateral variation of apparent resistivity values at a defined depth. These maps indicate the distribution of apparent resistivity in the area against distance of current electrodes. Interpretation of these maps was based on lithology and where there is low value of resistivity is considered as a dominant clayey or saturated material; while where there is high value of resistivity is considered as an aquifer made of gravel or as sandy dry material. For this step, sixteen maps where drawn, but only Six maps are presented base on change observed, respectively at AB/2 = 1.5; 13.2; 24.8; 40; 70 and 90 m.

3.3. Geohydraulic Parameters

The various parameters Hydraulic conductivity (K), Transmissivity (T), Porosity (Ø) and Longitudinal conductance (Lc) are obtained, based on true resistivity and thickness of aquifer after modelling VES data. These geohydraulic parameters are used to estimate the potential and protective capacity of different identified aquifers. Indirect calculation methods have been proposed by Oguama et al. (2020), Heigold et al. (1979) and Niwas and Singhal (1981) for basement area. However, recent studies conducted by many authors (Ibuot et al., 2022; Obiora & Ibuot, 2020; Oluchi et al., 2024) to determine the values of these parameters for a given aquifer (Equations (2)-(6)), show that these equations are applicable in sedimentary areas. This is done on condition that a calibration has been made between a borehole and a lithological section to determine the aquifer characteristics, as carried out in this study (**Figure 3**). Assessment of the aquifer vulnerability was done through determination of hydraulic conductivity of the aquifer protective layers. Its value is expressed in metres per day (m/day) and is obtained from Equation (2).

$$K = 386.40 Rw^{-0.93283} \tag{2}$$

where Rw is the resistivity of the aquifer in Ohm·m (Ω·m).

Hydraulic conductivity (K) is the ability of a porous medium to allow a fluid to pass through it under the effect of a pressure gradient. Aquifer vulnerability index (AVI) where describes as a right method to quantifies vulnerability by calculation of hydraulic resistance (C) to vertical flow of water through the covering layers (Stempvoort et al., 1993). The estimation of AVI requires to use two parameters to determine hydraulic resistance (C): the estimated hydraulic conductivity (Ki) and

the thickness (hi) of the protective layers. C was computed by using Equation (3):

$$C = \sum_{i=0}^{n}\left(\frac{hi}{Ki}\right) \tag{3}$$

After hydraulic resistance (C) obtained, values were compared to those in Table 1 which gives the relationship between C and AVI and helps to determine the level of vulnerability.

Table 1. Relationship between C and AVI after Stempvoort et al. (1993).

Hydraulic resistance (C)	Log C	Aquifer Vulnerability Index (AVI)	Level
0 - 10	<1	Extremely high	I
10 - 100	1 - 2	High	II
100 - 1000	2 - 3	Moderate	III
1000 - 10,000	3 - 4	Low	IV
>10,000	>4	Extremely low	V

The transmissivity (Tr) of an aquifer represents its capacity to mobilise the water it contains. It is a parameter that governs the rate of water flow per unit width of an aquifer (h), under the effect of the hydraulic gradient (K). Its value is expressed in metres square per day (m^2/day) and is obtained from Equation (4).

$$Tr = K\,x\,h \tag{4}$$

Computed transmissity values were comparing to standards (Table 2) classification proposed by Krasny (1993).

Table 2. Classification of *T magnitude* of Krasny.

Coefficient of Tr (m^2/day)	*Tr magnitude Class*	*Designation of Tr magnitude*	*Groundwater supply potential*
>1000	I	Very high	Withdrawals of great regional importance
1000 - 100	II	High	Withdrawals of lesser regional importance
100 - 10	III	Intermediate	Withdrawal for local water supply
10 - 1	IV	Low	Smaller withdrawal for local water supply
1 - 0.1	V	Very Low	Withdrawal for local water supply with limited consumption
<0.1	VI	Imperceptible	Source for local water supply is difficult

Longitudinal conductance (S in mhos) is a geoelectric parameter used to assess the protective capacity of the aquifer. It is expressed as results obtained by the ratio of the thickness of the aquifer (h in m) and the resistivity through Equation (5).

$$S = h/Rw \tag{5}$$

Longitudinal conductance is a crucial parameter in assessment of groundwater potential target. Its help to assess the protective capacity of an aquifer through

comparison between values obtained and those given in **Table 3** (Nwachukwu et al., 2019). Spatialization of this parameter in a given area helps identify areas with good groundwater potential to those with poor groundwater potential.

Porosity (Ø) expressed in %, is the percentage of voids per unit volume in a sediment or rock. It is deduced from Equation (6).

$$\varnothing = 25.5 + 4.5 \ln K \tag{6}$$

where K is the conductivity of the aquifer in m/day.

Table 3. Classification of protective capacity based on S rating.

Longitudinal Conductance (*mhos*)	*Protective capacity*
>10	Excellent
5 - 10	Very good
0.7 - 4.99	Good
0.2 - 0.69	Moderate
0.1 - 0.19	Weak
<0.1	Poor

All geohydraulic parameters obtained were spatialized and discussed in agreement with studies carried out in a similar context with regard to the difficulty of validation by pumping tests in the aquifers, given that many boreholes drilled tap several aquifers. However, the aquifer vulnerability index deduced from the geohydraulic parameters and used to determine the vulnerable zones by spatialization, were validated on the basis of known previous study (Akoachere et al., 2019; Emvoutou et al., 2018; Ketchemen Tandia, 2011; Ketchemen Tandia et al., 2017; Tchameni, 2020) and observations on the field in August 2022.

4. Results and Discussions

4.1. Piezometric Monitoring and Vulnerability Period

Based on the dynamics of the water table, the piezometric monitoring enabled classification into 5 periods: January to February; March to June; July to September; October to November and December. The variation in static levels and piezometric values recorded during piezometric monitoring allow to produce two maps. Examination of the piezometric maps show that the onset of rainfall at the end of February led to an increase in the piezometric depression and the multiplication of piezometric domes following the infiltration of water. The piezometric level rise from 23 m in January to 28 m in February, an increase of 5 m marking the end of the low-water period. Low water peaked in January (**Figure 4(a)**). During the period from March to June, numerous rainfall events gradually led to saturation of the ground by infiltration, resulting in the stabilisation of the piezometric level at 28 m and an increase in the volume of the depression and the piezometric domes. During the period from July to August, the intensity of rainfall al-

most tripled, and the piezometric level reached 30 m, recharging the water table. The piezometric maps show that the volume of the piezometric domes is at its maximum. This period of high water in the basin reaches its peak in August (Figure 4(b)).

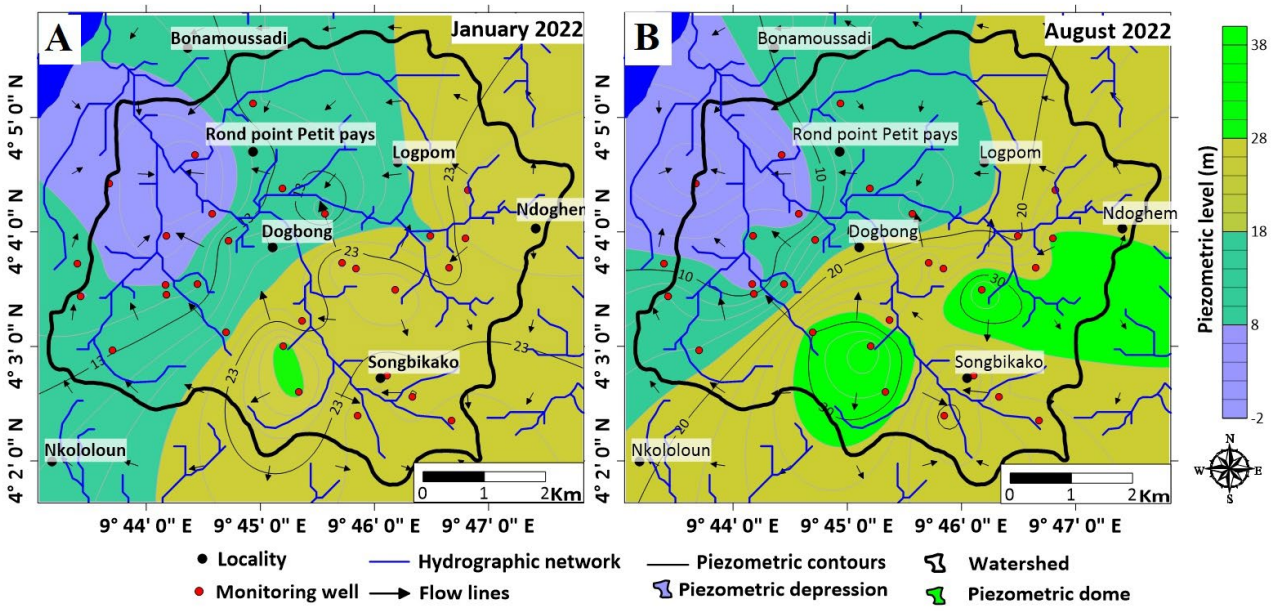

Figure 4. Piezometric maps (A) in dry and (B) rainy periods.

In the field, epidermal run-off and upwelling of more than 30 cm above the surface were observed, resulting in the widening and persistence of marshy areas. Rainfall became scarce between November and October, marking the end of the high-water period in the basin. The water table begins to empty, a process that continues until December, when the dry season begins. The maps illustrate the regression of the piezometric domes and in the field we can see a gradual regression until the marshy areas disappear. Analysis of the static levels shows that some wells reacted suddenly as soon as the first rains began in February, while others reacted late or slowly. The sudden rises reflect areas of low porosity and high permeability: these areas would be the most vulnerable, unlike the areas with late rises as suggested Ketchemen Tandia (2011), and Tchameni (2020). This rapid infiltration of rainwater contributes not only to the direct recharge of the water table but also to its pollution through the contribution of organic and mineral matter from the surface or effluents of waste waters (Akoachere et al., 2019; Emvoutou et al., 2018; Fantong et al., 2016; Ketchemen Tandia et al., 2017; Ngo Boum et al., 2015; Takem et al., 2015). The beat of the Tongo-Bassa water table is punctuated by alternating seasons. The fluctuating height of the groundwater varies from 0 m to 1.4 m in the wet and dry seasons respectively. The piezometric map of the Tongo-Bassa catchment show two sides: West side with very low piezometric levels and East side with high values of piezometric levels. Based on previous study cited

above, all wells of this West side are the most vulnerable to the nitrate and bacteriological pollution than those located at the East side where piezometric level are high. Only the wells located in the centre of this catchment have an average piezometric level. According to Akoachere et al. (2019) and Nlend et al. (2021), many factors, including the thickness of the unsaturated zone and the depth of the piezometric surface, plays a key role in the time to takes for a pollutant to be transferred to the water table. As the depth of the piezometric surface in the study area is shallow, groundwater pollution will be very rapid. The Tongo-Bassa soils are mainly composed of sands, clays and silts; so pollution is highly variable. The communication between the groundwater recharge zones (piezometric domes) in the South and South-East and the piezometric depressions in the North-West with the groundwater, accentuates the vulnerability of the latter, as these areas are densely populated. In the Douala V district, 56% of households dispose of wastewater in the open, 54.52% of households dispose of rubbish in the open and 14% dispose of rubbish in fields or ravines (Djuissi Tekam et al., 2019). Recharge of the Tongo-Bassa water table during rainfall by infiltration into accumulation zones is accompanied by pollution of the latter by transport and dissolution of these multiple mineral and organic pollutants. For the population, the various rivers in the catchment area are a receptacle for various types of waste and excreta. Water pollution in this case is influenced by hydrogeochemical and anthropogenic processes (Akoachere et al., 2019; Emvoutou et al., 2018; Njueya et al., 2012).

4.2. Spatial Variation of Apparent Resistivity

The maps (six) resulting from the data processing (**Figure 5**) have apparent resistivity values ranging from 19.46 to 98136.5 Ω·m, and are divided into three domains:

- conductive domain, with low apparent resistivity (19.46 to 2862.5 Ω·m) and represented by area with blue color;
- intermediaries domains with medium apparent resistivity (203.2 to 24285.7 Ω·m), and represented by yellow to orange color;
- resistive domain, with medium apparent resistivity (403.98 to 98136.5 Ω·m), and represented by red color.

Observation of the iso-resistivity maps (**Figure 5**) reveals that the different resistivity classes show a change in the resistivity field as you go deeper. **Figure 5** show six maps that better expresses lateral variation of the apparent resistivity at different depths in the study area, with two mains parts (North-Eastern and South-Western parts) in function of resistivity from surface (AB/2 = 1.5 m) to depth (AB/2 = 90 m). In general, South-Western part have low apparent resistivity values while North-Eastern part have high apparent resistivity. The zone with moderate resistivity values covers the centre and most of the sector.

Base on correlation with borehole logs (**Figure 3**) and previous study made by Ketchemen Tandia (2011), conductive areas with resistivity less than 200 Ω·m are made of Clay or Clayey sand material; while on this same domain, when resistivity

belongs to 200 to 800 Ω·m, material are made of Sandy clay or Sand. When resistivity is over 800 Ω·m, materials are essentially medium to coarse Sand.

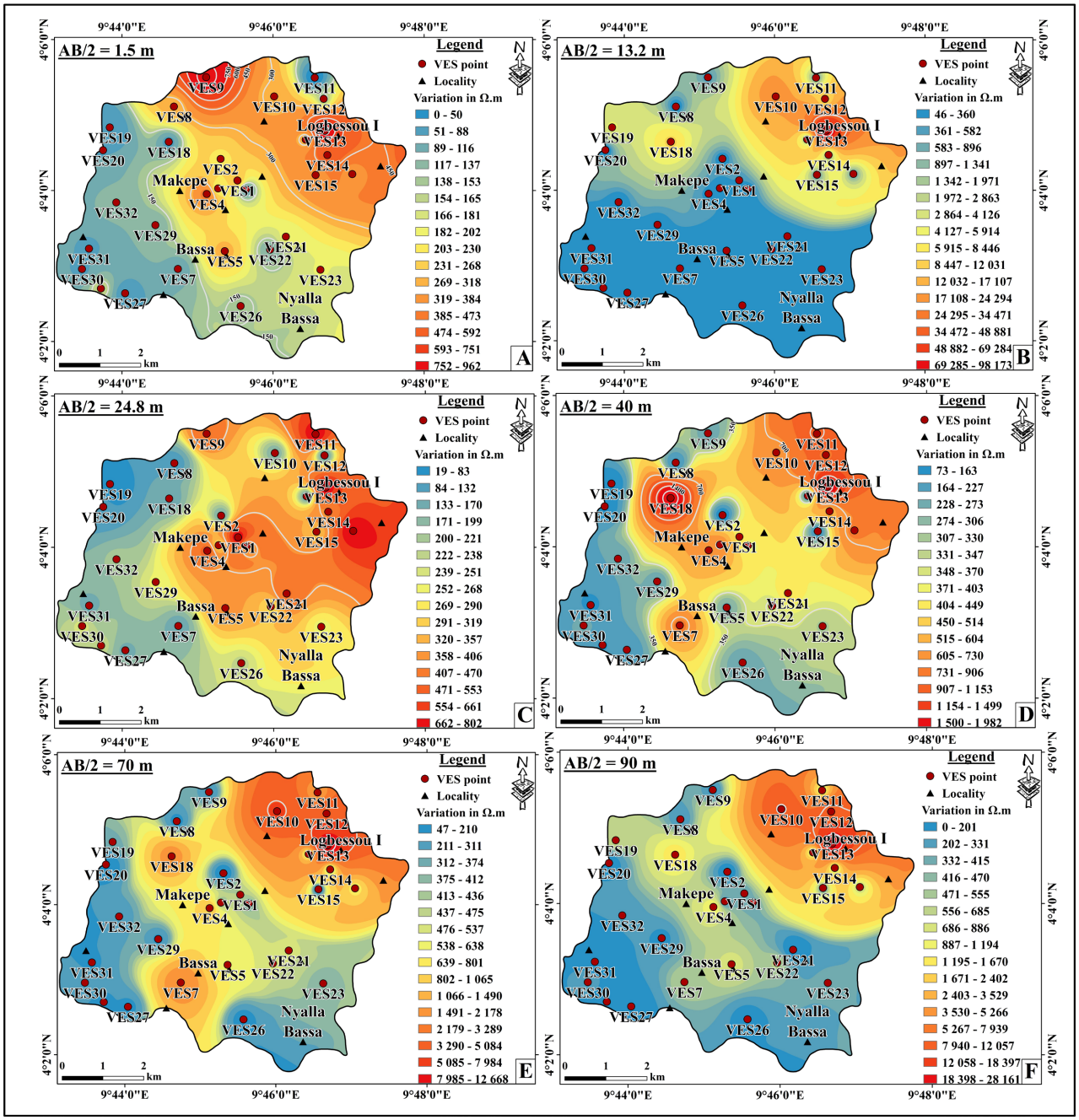

Figure 5. Apparent iso-resistivity maps at different investigation depths.

This observation implies that the North-Eastern part of watershed are sandier than the South-Western part; so, these areas should be more adapted to find sandy aquifers. The validation of this results was made with litho-logs of many boreholes (Bependa (Dla34), polyplast (Dla 8), Tropic (Dla9), Unalor (Dla 13) and CCC (Dla17) studied by Ketchemen Tandia, 2011) and new borehole drilled at Makepe,

in this area.

4.3. Curves Types and Aquifers Structure

Interpretation of the 1D inversion of the VES data revealed 10 mains types of curves (Table 4) and grouped as: HK (39.39%); KH (15.15%); 12.12% of HA and HKH; H (6.06%) while 3.03% represents K, AK, QH, KQ, and HKQ. Sounding data show three (H and K) to five geo-electric layers (HKH and HKQ).

Table 4. Synthesis of measured electrical resistivity data in the study area after inversion.

VES Code	Layers resistivity					Layers thickness				Curve Type
	ρ_1	ρ_2	ρ_3	ρ_4	ρ_5	h_1	h_2	h_3	h_4	
VES27	57.45	114.1	410.4	6.358		1.662	10.97	29.81		AK
VES22	166	8.08	9980			0.935	1.08			H
VES28	2453	87.99	172.7			0.3293	1.784			
VES4	3716	142	234	1689		0.404	0.987	6.07		HA
VES7	112	35	870	7200		1.05	2.1	38.2		
VES16	2570	24.98	33.95	479		0.4231	0.4128	3.777		
VES23	8458	35.9	283	477		0.295	0.652	13.6		
VES1	874	28.5	4250	158		0.579	0.557	3.97		HK
VES2	591.5	21.2	957.2	33.31		0.625	0.883	2.572		
VES6	8236	51.91	1258	3.26		0.28	4.456	6.66		
VES11	4830	64.5	8700	56.6		0.5	1.43	8.12		
VES14	2091	144.1	2912	50.21		0.503	7.297	7.636		
VES17	79.44	39.43	935.5	202.9		1.157	1.095	14.24		
VES20	7409	32.99	242.8	18.3		0.2682	4.976	10.08		
VES24	4312	40.51	7000	55		0.3931	0.8997	5		
VES25	861	44.99	1196	15.73		0.436	3.347	15.04		
VES26	2313	94.74	610	21.48		0.296	5.23	12.42		
VES29	365	19.6	2416	104		0.561	0.941	2.28		
VES30	564	11.6	753	16.8		0.45	1.04	25.2		
VES32	939.4	40.83	497.4	18.12		0.41	2.994	24.87		
VES3	2857	30.6	1989	30.7	5300	0.38	0.8	2.23	15.5	HKH
VES5	1327	39.56	1990	138.8	7900	0.502	0.854	1.994	16.57	
VES15	2089	122.6	493.1	39.73	5078	0.42	1.49	10.27	20.06	
VES31	294.9	23	1216	72.62	383	0.493	1.02	1.57	15.8	
VES9	4662	170.7	1673	418.3	104.6	0.42	0.59	1.525	18.31	HKQ
VES21	167	592	383			1.82	12.9			K

Continued

VES10	296	4810	808	7924	0.9	3.4	17.4	
VES12	75	6230	274	7984	1.67	3.24	14.1	
VES13	1143	7246	648	790	0.9	1.07	2.34	KH
VES18	153	3540	97.1	6647	0.81	1.04	7.28	
F1	125.4	5127	176.2	482.4	0.9	1.185	10.98	
VES19	61.31	3537	220	96.29	0.7965	1.079	0.9619	KQ
VES8	484.5	105.6	88.69	5200	0.635	1.65	36	QH

4.4. Aquifers Potentiality and Protectivity

Base on the analysis of VES data and curve type with lithology, two main aquifers are identified: first aquifer made of unconfined aquifer, and second one made of semi-confined or confined aquifer. These two aquifers are used by population through open wells or boreholes. Then their potentiality and protective capacity in the study area was evaluated by geohydraulic parameters, and the results are analysed separately with illustration of their spatial variation.

4.4.1. Case of Unconfined Aquifer

Geohydraulic parameters (porosity ϕ, hydraulic conductivity K, transmissivity Tr, longitudinal conductance S, and hydraulic resistance C) of the unconfined aquifer were estimated (**Table 5**) using the combination of resistivity and thickness through Equations (2)-(6). The AVI was determined in term of Log C to assess the level of vulnerability. Aquifer resistivity and thickness of this unconfined aquifer ranged from 57.45 to 8458 Ω·m and 0.30 to 12.9 m respectively. The low value of resistivity can be explained by the presence of argillaceous formation facies which combine to weak thickness may lower the aquifer potentials like shows many authors (Obiora et al., 2016; Nwachukwu et al., 2019; Obiora & Ibuot, 2020).

High resistivity values combine to sandy formations which combine to very thick layers show great aquifer potentials. Porosity range from 14.35 to 35.30%; hydraulic conductivity from 0.08 to 8.83 m/day; longitudinal conductance from $3.4 * 10^{-5}$ to 0.0289 mhos; transmissivity from 0.02 to 14.67 m^2/day; and hydraulic resistance from 0.265 to 29.29 day^{-1}. These parameters in accordance to standards (**Table 1**, **Table 2** and **Table 3**) show that these unconfined aquifers are extremely vulnerable (87.88%) and groundwater supply potential are fairly adapted for local level with limited consumption for private water supply due to less permeable materials or discontinuous aquifer formations (Obioma et al., 2024). In comparison to study made by Javed et al. (2024), average yields of this aquifer can be estimated as less than 6 l/s for 51.51% of data, and ranged between 6 - 30 l/s, for 36.36% of data. Spatialization by kriging method, shows a contour map displaying the distribution of these geohydraulic parameters (**Figure 6**) which divide watershed in two particular domains:

- North to North-Eastern domain, which have weak geohydraulic values; and

- South to South-western domain with high geohydraulic values.

Table 5. Estimated geohydraulic parameter for the unconfined aquifer.

VES code	Rw (Ω·m)	h (m)	K (m/day)	Ø (%)	S (Ω^{-1}) *10^{-3}	Tr (m^2day)	Tr Class	C_1 (day^{-1})	LogC_1	AVI
VES1	874	0.58	0.70	23.87	0.66	0.40	V	0.86	−0.06	
VES2	591.5	0.63	1.00	25.51	1.06	0.63		0.66	−0.18	
VES3	2857	0.38	0.23	18.90	0.13	0.09	VI	1.70	0.23	
VES4	3716	0.40	0.18	17.80	0.11	0.07		2.50	0.40	
VES5	1327	0.50	0.47	22.12	0.38	0.24	V	1.13	0.05	Extremely High
VES6	8236	0.28	0.09	14.46	0.03	0.02	VI	3.72	0.57	
VES7	112	1.05	4.74	32.50	9.38	4.97	IV	0.37	−0.43	
VES8	484.5	0.64	1.21	26.35	1.31	0.77	V	0.86	−0.07	
VES9	4662	0.42	0.15	16.85	0.09	0.06	VI	3.06	0.49	
VES10	4810	3.40	0.14	16.72	0.71	0.48	V	24.42	1.39	High
VES11	4830	0.50	0.14	16.70	0.10	0.07	VI	3.72	0.57	Extremely High
VES12	6230	3.24	0.11	15.63	0.52	0.36		29.29	1.47	High
VES13	7246	1.07	0.10	15.00	0.15	0.10		12.70	1.10	
VES14	2091	0.50	0.31	20.21	0.24	0.16	V	3.58	0.55	
VES15	2089	0.42	0.31	20.22	0.20	0.13		1.70	0.23	
VES16	2570	0.42	0.25	19.35	0.17	0.11		1.68	0.23	
VES17	79.44	1.16	6.53	33.94	14.56	7.55	IV	0.26	−0.58	Extremely High
VES18	3540	1.04	0.19	18.00	0.29	0.20	V	5.73	0.76	
VES19	3537	1.08	0.19	18.01	0.31	0.20		5.80	0.76	
VES20	7409	0.27	0.09	14.90	0.04	0.03	VI	3.16	0.50	
VES21	592	12.9	1.00	25.51	21.79	12.93	III	13.43	1.13	High
VES22	166	0.94	3.28	30.85	5.63	3.07	IV	0.30	−0.52	
VES23	8458	0.30	0.08	14.35	0.04	0.02	VI	3.57	0.55	Extremely High
VES24	4312	0.39	0.16	17.17	0.09	0.06		2.57	0.41	
VES25	861	0.44	0.71	23.94	0.51	0.31	V	0.92	−0.04	
VES26	2313	0.30	0.28	19.79	0.13	0.08	VI	2.00	0.30	
VES27	57.45	1.66	8.83	35.30	28.93	14.67	III	2.54	0.41	
VES28	2453	0.33	0.27	19.54	0.13	0.09	VI	1.54	0.19	
VES29	365	0.56	1.57	27.54	1.54	0.88		0.40	−0.40	Extremely High
VES30	564	0.45	1.05	25.71	0.80	0.47		0.46	−0.34	
VES31	294.9	0.49	1.92	28.43	1.67	0.95	V	0.31	−0.51	
VES32	939.4	0.41	0.65	23.57	0.44	0.27		0.88	−0.06	
F1	5127	1.19	0.13	16.45	0.23	0.16		9.07	0.96	

The different maps obtained through spatialization, show that groundwater potential decreasing from this South and South-Western domain, to North and North-Eastern domain; while AVI increasing in the same direction.

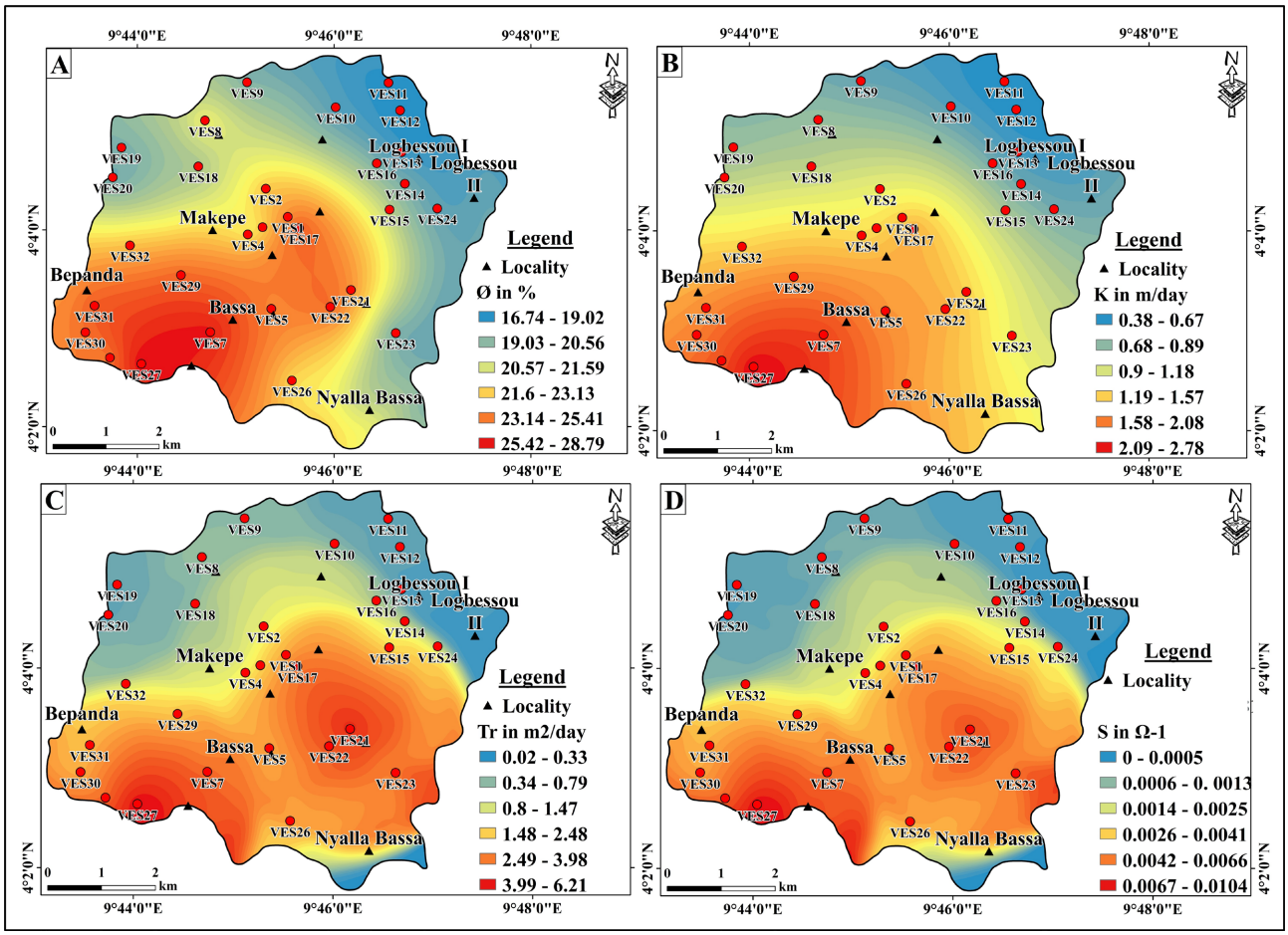

Figure 6. Spatial variation of geohydraulic parameters of unconfined aquifer (A) porosity; (B) conductivity, (C) transmissivity; (D) longitudinal conductance.

4.4.2. Case of Semi-Confined/Confined Aquifer

In second aquifer level identify after VES computing, many geohydraulic parameter has varying as presented in **Table 6** while the graphical presentation depicting the spatial variations of some of these geohydraulic parameters with respect to VES points shown in **Figure 7**. Resistivity and thickness ranged from 172.7 (VES 28) to 9980 Ω·m (VES 22) and from 1 to 38.2 m respectively. Porosity and Hydraulic conductivity values ranged from 13.65 to 30 % and from 0.072 to 3.16 m/day respectively. Spatial distribution of these two parameters over the study area (**Figure 7(A)** and **Figure 7(B)**) indicated that the western and eastern part, had a high value, implying ability of these section to get a high groundwater potential which can move easily through the pore spaces. According to Udosen et al. (2024), space of a given area with high value of hydraulic conductivity can be linked to the space with a high groundwater potential and where there is a great

level of hydraulic flow and groundwater recharge. Conversely the center part of the study area showing low values of hydraulic conductivity, implying low groundwater potential and difficulties of groundwater flowing and recharge. Based on the study made by Javed et al. (2024), 33.34% of data could had yield less than 6 l/s due to K < 0.3 m/day; while 63.64% should have yield ranged between 6 - 30 l/s. In the Tongo-Bassa watershed, transmissivity values of confined or semi-confined aquifer ranged from 0.077 m^2/day to 42.04 m^2/day, with an average of 7.606 m^2/day. Wide range of transmissivity show high heterogeneities of lithology and groundwater potential and flowing. Classification of this transmissivity in the study area show that this aquifer is adapted for groundwater supply for small communities at local scale for 72.73% of data and more represented in Southern sector (**Figure 7(C)**), while 27.27% of data are adapted for private water supply in Northern sector. Longitudinal conductance which is a key geohydraulic parameter used to assess the protective capacity of aquifers, ranged from 0.00011 to 0.0726 Ω^{-1} with average of 0.0128 Ω^{-1}. This longitudinal conductance confirms also poor protective capacity, in line with AVI which remain High to Extremely high (excepted VES 11 which show a moderate AVI), compared to results obtained in the same environments at the Southern side of Benue State in Nigeria (Eyankware et al., 2021), where good protective capacity of deep and confined aquifer were observed. **Figure 7(D)** shows that Northern part of the watershed (in blue color), near the west part of the outlet, are more vulnerable.

These various maps showing a correlation between changes in porosity and permeability. In fact, the most porous areas are also the most permeable. However, the transmissivity maps are similar to those showing longitudinal conductance, where the areas with potential for rapid transmission are the least vulnerable. This contrast with previous hydrogeochemical studies in the area, where the most polluted wells were found by many authors (Emvoutou et al., 2018; Ketchemen Tandia, 2011; Ngo Boum et al., 2015). However, this contrast can be explained by the combined action of topography, slope and the nature of the material as suggested by Akoachere et al. (2019). In fact, if the high areas near the ridges are made up of sand, whereas the low areas are rich in clay, the action of the slope means that the water will circulate quickly upstream and slowly downstream, with water levels in the wells almost invariant in dry and rainy season. It goes without saying that the critical discrepancy between the low calculated vulnerability of the deep aquifer and the pollution observed in previous studies could be linked to the intertwined structure of the layers, which, due to lateral circulation as observed in piezometric studies, could bring the confined aquifer waters into contact with pollutants from surface waters. Similarly, this situation could be explained by the fact that on the field, when drilling wells, populations capture both surface and deep groundwater in order to obtain high flow rates; which makes the confined/semi-confined aquifer more vulnerable.

This means that if a pollutant is introduced into the environment, it will be rapidly transported laterally downstream, and when circulation is slow, the wells

analysed downstream will be more polluted than those upstream. This situation explains why in the study area, many polluted wells which exploited unconfined aquifer are identified where it's supposed to be less vulnerable while in the same environment, boreholes which exploited confined or semi-confined aquifer are less polluted due to their relative protection by clayey material.

Table 6. Estimated geohydraulic parameter for the semi-confined/confined aquifer.

VES code	Rw (Ω·m)	h (m)	K (m/day)	Ø (%)	S (Ω^{-1})*10^{-3}	Tr (m^2/day)	Tr Class	C2 (day^{-1})	LogC2	AVI
VES1	4250	3.97	0.16	17.24	0.9	0.63	V	25.78	1.41	High
VES2	957.2	2.57	0.64	23.49	2.70	1.65	IV	4.68	0.67	Extremely High
VES3	1989	2.23	0.32	20.42	1.10	0.72	V	8.59	0.93	
VES4	1689	6.07	0.38	21.11	3.60	2.29	IV	5.04	0.70	
VES5	1990	16.57	0.32	20.42	8.30	5.36	IV	7.30	0.86	
VES6	1258	6.66	0.50	22.35	5.30	3.30	IV	17.14	1.23	High
VES7	7200	38.2	0.10	15.02	5.30	3.72	IV	54.96	1.74	
VES8	5200	36	0.13	16.39	6.90	4.75	IV	6.97	0.84	Extremely High
VES9	1673	1.53	0.38	21.15	0.90	0.58	V	7.07	0.85	
VES10	7924	17.4	0.09	14.62	2.20	1.55	IV	47.63	1.68	High
VES11	8700	8.12	0.08	14.23	0.90	0.66	V	103.12	2.01	Moderate
VES12	7984	14.1	0.09	14.59	1.80	1.25	IV	36.15	1.56	High
VES13	790	2.34	0.77	24.30	3.00	1.79	IV	15.24	1.18	
VES14	2912	7.64	0.23	18.82	2.60	1.73	IV	37.25	1.57	
VES15	493.1	10.27	1.19	26.28	20.80	12.21	III	10.34	1.01	
VES16	479	3.78	1.22	26.40	7.90	4.61	IV	1.94	0.29	Extremely High
VES17	935.5	14.24	0.65	23.59	15.20	9.31	IV	22.04	1.34	High
VES18	6647	7.28	0.10	15.36	1.10	0.76	V	7.08	0.85	Extremely High
VES19	220	0.96	2.52	29.66	4.40	2.43	IV	6.18	0.79	
VES20	242.8	10.08	2.30	29.25	41.50	23.20	III	7.54	0.88	
VES21	383	12.9	1.50	27.34	33.70	19.41	III	22.01	1.34	High
VES22	9980	10.8	0.07	13.65	1.08	0.78	V	15.33	1.19	
VES23	477	13.6	1.23	26.42	28.50	16.67	III	10.38	1.02	
VES24	7000	5	0.10	15.14	0.70	0.50	V	52.55	1.72	
VES25	1196	15.04	0.52	22.56	12.60	7.82	IV	29.84	1.47	
VES26	610	12.42	0.97	25.38	20.40	12.10	III	14.74	1.17	
VES27	410.4	29.81	1.41	27.05	72.60	42.05	III	23.68	1.37	
VES28	172.7	1.784	3.16	30.68	10.30	5.64	IV	2.10	0.32	Extremely High
VES29	2416	2.28	0.27	19.61	0.90	0.62	V	8.84	0.95	
VES30	753	25.2	0.80	24.50	33.50	20.18	III	31.93	1.50	High
VES31	1216	1.57	0.51	22.49	1.30	0.80	V	3.37	0.53	Extremely High
VES32	497.4	24.87	1.18	26.24	5.00	29.32	III	21.97	1.34	High
F1	482.4	10.98	1.21	26.37	22.80	13.32	III	12.61	1.10	

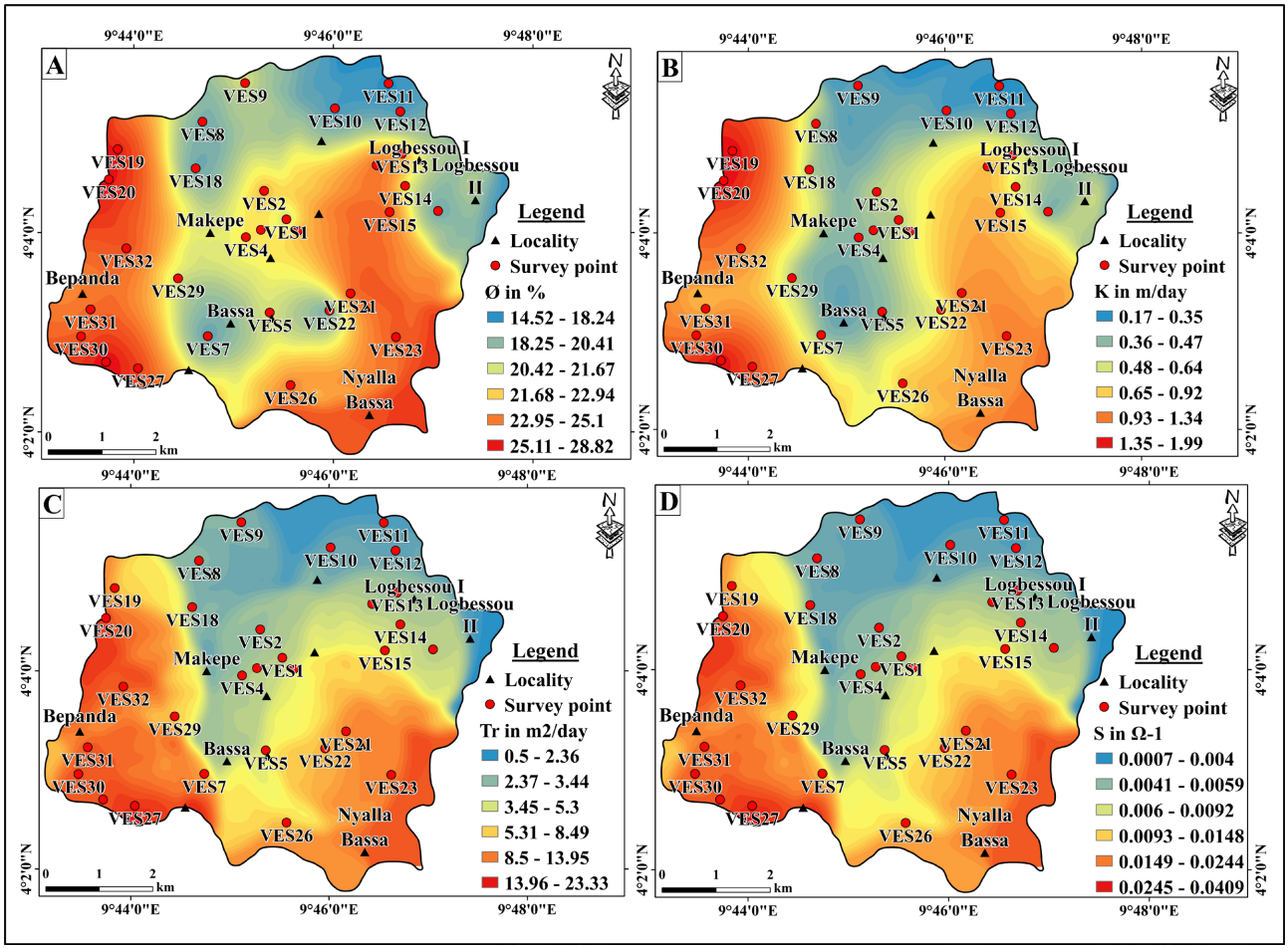

Figure 7. Spatial variation of geohydraulic parameters of confined/semi-confined aquifer (A) porosity; (B) conductivity; (C) transmissivity; (D) longitudinal conductance.

5. Conclusion

The Quaternary/Mio-Pliocene aquifer in Douala Sedimentary Basin (DSB) is solicited for groundwater supply. In order to help authorities manage well this important aquifer, its potential and vulnerability was evaluated through piezometric and geo-electrical surveys. Piezometric studies have shown an unconfined aquifer, with groundwater flowing towards the natural outlet in general, masking the structural heterogeneity of the terrain, which is apparent during the rainy season. Based on the flowing of groundwater in this unconfined aquifer in general, vulnerability increases from Southeastern to Northwestern direction. VES data after inversion and correlation with borehole logs allow to distinguish two aquifers: unconfined superficial aquifer (depth < 28 m), and deep semi-confined or confined aquifer (depth < 70 m). Primary parameters (resistivity and thickness) obtained after analysing VES data were used to determine geohydraulic parameters (porosity, hydraulic conductivity, transmissivity, longitudinal conductance and hydraulic resistance) in order to evaluate potential and vulnerability (AVI) of the two aquifers identified. Then, concerning vulnerability, unconfined and superfi-

cial aquifer is more vulnerable (−0.58 < Log C < 0.96) with 87.87% of the area, compared to the semi confined/confined aquifer (0.29 < Log C < 0.95) which show that only 39.39% of the area are vulnerable. About groundwater potential, unconfined aquifer has potential adapted for local level with limited consumption for private water supply (0.02 < Tr < 14.67 m^2/day), while confined/semi confined aquifer has a potential adapted to supply a small community at local scale (0.50 < Tr < 42.05 m^2/day). Realization of contour maps of the geohydraulic parameters indicate for these aquifers, where potential is high and where groundwater is more or less vulnerable to pollution. All parameters obtained provide information's in groundwater resource management as well as acts as a guide to assess the vulnerability of different hydrogeological units in DSB. These results illustrate the lithological and structural complexity of the DSB and its influence on groundwater potential, as well as on efficient management of the resource for better development planning. Based on the results obtained, we recommend that local authorities and individuals wishing to drill a well or borehole, should focus on deep groundwater from confined/semi-confined aquifers, which appear to be less vulnerable to pollution. Similarly, these populations should avoid mixing surface water with deep groundwater in order to preserve this precious resource.

Acknowledgements

The authors would like to express their deepest gratitude to the field team for the efforts made to enable successful data collection.

Conflicts of Interest

The authors declared that there were no conflicts of interest.

References

Akakuru, O. C., Onyeanwuna, U. B., Opara, A. I., Iheme, K. O., Njoku, A. O., Amadi, C. C. et al. (2023). Electro-Geohydraulic Estimation of Shallow Aquifer Characteristics of Njaba and Environs, Southeastern Nigeria. *Arabian Journal of Geosciences, 16,* Article No. 318. https://doi.org/10.1007/s12517-023-11378-1

Akoachere, R. A., Egbe, S. E., Eyong, T. A., Edimo, S. N., Longonje, S. N., Tambe, D. B. et al. (2019). Seasonal Variations in Groundwater of the Phreatic Aquiferous Formations in Douala City-Cameroon: Hydrogeochemistry and Water Quality. *OALib, 6,* 1-26. https://doi.org/10.4236/oalib.1105328

Amaneudjeu, A., (2019). *Analyse temporelle de la représentation du risque d'inondation de 1980 à 2018 à Douala-Cameroun.* Ph.D. Thesis, University of Liège.

Bentekhici, N., Benkesmia, Y., Berrichi, F., & Bellal, S. (2018). Assessing Water Pollution Risk and Groundwater Vulnerability Using Spatial Data. Case of the Sidi Bel Abbes plain (North-West Algeria). *Journal of Water Science, 31,* 43-59.

Djuissi Tekam, D., Vogue, N., Nkfusai, C. N., Ebode Ela, M., & Cumber, S. N. (2019). Accès à l'eau potable et à l'assainissement: Cas de la commune d'arrondissement de Douala 5ème (Cameroun). *Pan African Medical Journal, 33,* Article 244. https://doi.org/10.11604/pamj.2019.33.244.17974

Dumord, J. D. (1968). *Notice explicative sur la feuille Douala-Ouest. Carte géologique de reconnaissance (1/500000)* (p. 69). Publication Direction des Mines et de la Géologie du Cameroun.

El Kayssi, Y., Hilali, M., Kouz, T., & Kacimi, I. (2020). Évaluation de la vulnérabilité à la pollution des eaux souterraines par la méthode DRASTIC: Cas de la nappe alluviale de Rich (Haut Atlas central, Maroc). *Revue des Sciences de l'Eau, 32,* 317-334. https://doi.org/10.7202/1069568ar

Emvoutou, H. C., Ketchemen Tandia, B., Ngo Boum Nkot, S., Ebonji, R. C. S., Nlend, Y. B., Ekodeck, G. E. et al. (2018). Geologic Factors Controlling Groundwater Chemistry in the Coastal Aquifer System of Douala/Cameroon: Implication for Groundwater System Functioning. *Environmental Earth Sciences, 77,* Article No. 219. https://doi.org/10.1007/s12665-018-7400-z

Eyankware, M. O., Ogwah, C., & Star, U. O. (2021). Integrated Geophysical and Hydrogeochemical Characterization and Assessment of Groundwater Studies in Adum West Area of Benue State, Nigeria. *Journal of Geological Research, 3,* 12-25. https://doi.org/10.30564/jgr.v3i3.3197

Fantong, W. Y., Kamtchueng, B. T., Ketchemen-Tandia, B., Kuitcha, D., Ndjama, J., Fouepe, A. T. et al. (2016). Variation of Hydrogeochemical Characteristics of Water in Surface Flows, Shallow Wells, and Boreholes in the Coastal City of Douala (Cameroon). *Hydrological Sciences Journal, 61,* 2916-2929. https://doi.org/10.1080/02626667.2016.1173789

Feumba, R., (2015). *Hydrogéologie et évaluation de la vulnérabilité des nappes dans le Bassin Versant de Bessekè (Douala-Cameroun).* Master's Thesis, Université de Yaoundé I.

Gilli, E., Mangan, C., & Mudry, J. (2008). Hydrogéologie: Objets, Méthodes et Applications, 2ème Edition. Dunod.

Heigold, P. C., Gilkeson, R. H., Cartwright, K., & Reed, P. C., (1979). Aquifer Transmissivity from Superficial Electrical Method, Estimation of Aquifer Transmissivity from Dar-Zarrouks Parameters in Porous Media. *Groundwater, 17,* 338-345.

Hounsounou, E. O., Agassounon Djikpo Tchibozo, M., Kelome, N. C., Vissin, E. W., Mensah, G. A., & Agbossou, E. (2016). Pollution des eaux à usages domestiques dans les milieux urbains défavorisés des pays en développement: Synthèse bibliographique. *International Journal of Biological and Chemical Sciences, 10,* 2392-2412. https://doi.org/10.4314/ijbcs.v10i5.35

Ibuot, J. C., Aka, M. U., Inyang, N. J., & Agbasi, O. E. (2022). Georesistivity and Physicochemical Evaluation of Hydrogeologic Units in Parts of Akwa Ibom State, Nigeria. *International Journal of Energy and Water Resources, 8,* 111-122. https://doi.org/10.1007/s42108-022-00191-3

Ibuot, J. C., George, N. J., Okwesili, A. N., & Obiora, D. N. (2019). Investigation of Litho-Textural Characteristics of Aquifer in Nkanu West Local Government Area of Enugu State, Southeastern Nigeria. *Journal of African Earth Sciences, 153,* 197-207. https://doi.org/10.1016/j.jafrearsci.2019.03.004

Ibuot, J. C., Obiora, D. N., & George, N. J. (2024). Evaluation of Geohydraulic Response Properties of Hydrogeological Units in Littoral Hydro-Lithofacies in Uyo, Southern Nigeria. *Applied Water Science, 14,* Article No. 9. https://doi.org/10.1007/s13201-023-02057-3

Ibuot, J. C., Obiora, D. N., Ekpa, M. M. M., & Okoroh, D. O. (2017). Geoelectrohydraulic Investigation of the Surficial Aquifer Units and Corrosivity in Parts of Uyo L. G. A., Akwa Ibom State, Southern Nigeria. *Applied Water Science, 7,* 4705-4713. https://doi.org/10.1007/s13201-017-0632-3

Igboama, W. N., Hammed, O. S., Fatoba, J. O., Aremu, I. E., & Aroyehun, M. T. (2021). Geo-electric and Hydro-Physiochemical Investigations of Osogbo Central Dumpsite, Osogbo, Southwestern Nigeria. *Arabian Journal of Geosciences, 14,* Article No. 361. https://doi.org/10.1007/s12517-021-07766-0

Javed, U., Kumar, P., Hussain, S., Nawaz, T., Fahad, S., Ashraf, S. et al. (2024). Geospatial Analysis of Soil Resistivity and Hydro-Parameters for Groundwater Assessment. *Discover Geoscience, 2,* Article No. 3. https://doi.org/10.1007/s44288-024-00004-6

Ketchemen Tandia, B. (2011). *Déterminants hydrogéologiques de la complexité du système aquifère du bassin sédimentaire de Douala (Cameroun).* Master's Thesis, Faculté des Sciences et Techniques, Université Cheikh Anta Diop de Dakar.

Ketchemen-Tandia, B., Boum-Nkot, S. N., Ebondji, S. R., Nlend, B. Y., Emvoutou, H., & Nzegue, O. (2017). Factors Influencing the Shallow Groundwater Quality in Four Districts with Different Characteristics in Urban Area (Douala, Cameroon). *Journal of Geoscience and Environment Protection, 5,* 99-120. https://doi.org/10.4236/gep.2017.58010

Krasny, J. (1993). Classification of Transmissivity Magnitude and Variation. *Groundwater, 31,* 230-236. https://doi.org/10.1111/j.1745-6584.1993.tb01815.x

Mbesse, C., (2014). *La limite Paléocéne-Eocéne dans le bassin de Douala Biostratigraphie et essai de reconstituion des paléoenvironement.* Master's Thesis, University of Yaoundé I.

Mbog, M. B., Kenfack, J. V., Ngon, G. F., Tassongwa, B., Bayiga, E. C., & Etame, J. (2019). Morpho-structural Mapping Constraints from Geophysical and Test Pit Investigations: Case Study of the Bomkoul Locality in Douala Sedimentary Basin, Cameroon, Central Africa. *Journal of Geoscience and Environment Protection, 7,* 136-153. https://doi.org/10.4236/gep.2019.710011

Mvondo, O. F. (2010). *Surrection cénozoïque de l'Ouest de l'Afrique à partir de deux exemples: Le plateau sud namibien la marge nord camerounaise.* Master's Thesis, Université de Rennes.

Ndjigui, P., Bilong, D. P., Nyek, B., Eno, B. S. M., & Gerad, M. (1999). Etude morphologique, minéralogique et géochimique de deux profils latéritiques dans la plaine de Douala (Cameroun). In J. P. Vicat & P. Bilong (Eds.), *Géologie et environnement au Cameroun* (pp. 189-201). Collection Geocam Press, UNIVERSITé de Yaoundé I.

Ngo Billong, P. T., Feumba, R., & Ndjigui, P. (2023). Hydrogeochemical Appraisal of Groundwater Quality in Ngoua Watershed (Douala-Cameroon): Implication for Domestic Purposes. *Scientific African, 22,* e01910. https://doi.org/10.1016/j.sciaf.2023.e01910

Ngo Boum, N. S., Ketchemen Tandia, B., Ndje, Y., Emvoutou, H., Ebonji Seth, C. R., Huneau, F. (2015). Origin of Mineralization of Groundwater in the Tongo Bassa. *Journal of Hydrogeology and Hydrologic Engineering, 4,* Article 1. https://doi.org/10.4172/2325-9647.1000117

Nguene, F. R., Tamfu, S., Loule, J. P., & Ngassa, C. (1992). Paleoenvironment of the Douala and Kribi/Campo Sub Basins in Cameroon West Africa. In *1er Colloque de Stratigraphie et de Paléogéographie des Bassins Sédimentaires Ouest-Africains, 2ème Colloque Africain de Micropaléontologie* (pp. 129-139). Libreville.

Ngueutchoua, G. (1996). *Etude des faciès et environnement sédimentaire du Quaternaire supérieur du plateau continental Camerounais.* Master's Thesis, Université de Perpignan Via Domitia.

Niwas, S., & Singhal, D. C. (1981). Estimation of Aquifer Transmissivity from Dar-Zarrouk Parameters in Porous Media. *Journal of Hydrology, 50,* 393-399.

https://doi.org/10.1016/0022-1694(81)90082-2

Njiké Ngaha, P. R. (2004). *Palyno-stratigraphie et reconstitution des paléoenvironnements du Crétacé de l'Est du bassin sédimentaire de Douala (Cameroun).* Master's Thesis, Université de Yaoundé I.

Njueya, A., Likeng, J., & Nono, A. (2012). Hydrodynamique et qualité des eaux souterraines dans le bassin sédimentaire de Douala (Cameroun): Cas des aquifères sur formations Quaternaires et Tertiaires. *International Journal of Biological and Chemical Sciences, 6,* 1874-1894. https://doi.org/10.4314/ijbcs.v6i4.41

Nlend, B., Celle-Jeanton, H., Huneau, F., Garel, E., Boum-Nkot, S. N., & Etame, J. (2021). Shallow Urban Aquifers under Hyper-Recharge Equatorial Conditions and Strong Anthropogenic Constrains. Implications in Terms of Groundwater Resources Potential and Integrated Water Resources Management Strategies. *Science of the Total Environment, 757,* Article ID: 143887. https://doi.org/10.1016/j.scitotenv.2020.143887

Nsegbe, A. (2021). Pression urbaine et état de santé de l'environnement de Makepe-Missoke, un ancien front d'urbanisation dans l'arrondissement de Douala 5ème (Cameroun). *Mutation environnemental et risque sanitaire en afrique, 4,* 7.

Nwachukwu, S., Bello, R., & Balogun, A. O. (2019). Evaluation of Groundwater Potentials of Orogun, South-South Part of Nigeria Using Electrical Resistivity Method. *Applied Water Science, 9,* Article No. 184. https://doi.org/10.1007/s13201-019-1072-z

Obioma A. S., Odochi U. B., Ezenwa O. Y., Chukwuemeka I. C., & Chinyere C. A. (2024). Geoelectrical Resistivity Mapping for Sustainable Groundwater Management in Umuahia South: Insights from Vertical Electrical Sounding. *International Journal of Science and Research Archive, 13,* 2296-2319. https://doi.org/10.30574/ijsra.2024.13.1.1922

Obiora, D. N., & Ibuot, J. C. (2020). Geophysical Assessment of Aquifer Vulnerability and Management: A Case Study of University of Nigeria, Nsukka, Enugu State. *Applied Water Science, 10,* Article No. 29. https://doi.org/10.1007/s13201-019-1113-7

Obiora, D. N., Ajala, A. E., & Ibuot, J. C. (2015). Evaluation of Aquifer Protective Capacity of Overburden Unit and Soil Corrosivity in Makurdi, Benue State, Nigeria, Using Electrical Resistivity Method. *Journal of Earth System Science, 124,* 125-135. https://doi.org/10.1007/s12040-014-0522-0

Obiora, D. N., Ibuot, J. C., & George, N. J. (2016). Evaluation of Aquifer Potential, Geoelectric and Hydraulic Parameters in Ezza North, Southeastern Nigeria, Using Geoelectric Sounding. *International Journal of Environmental Science and Technology, 13,* 435-444. https://doi.org/10.1007/s13762-015-0886-y

Oguama, B. E., Ibuot, J. C., & Obiora, D. N. (2020). Geohydraulic Study of Aquifer Characteristics in Parts of Enugu North Local Government Area of Enugu State Using Electrical Resistivity Soundings. *Applied Water Science, 10,* Article No. 120. https://doi.org/10.1007/s13201-020-01206-2

Oli, I. C., Ahairakwem, C. A., Opara, A. I., Ekwe, A. C., Osi-Okeke, I., Urom, O. O. et al. (2020). Hydrogeophysical Assessment and Protective Capacity of Groundwater Resources in Parts of Ezza and Ikwo Areas, Southeastern Nigeria. *International Journal of Energy and Water Resources, 5,* 57-72. https://doi.org/10.1007/s42108-020-00084-3

Oluchi, E. C., Ngozi, O. M., & Ibuot, J. C. (2024). Aquifer Vulnerability Studies Using Electrical Resistivity Method in Nsukka East and West Local Government Area, Enugu State, Nigeria. *Geological Behavior, 8,* 38-47. https://doi.org/10.26480/gbr.01.2024.38.47

Orellana, E., & Mooney, H. M. (1966). Master Tables and Curves for Vertical Electrical Sounding over Layered Structures. Interciencia, Costanilla de Los Angeles, 15, Madrid.

Regnoult, J. (1986). *Synthèse géologique du Cameroun* (p. 119). Ministère des Mine, Ya-

oundé-Cameroun.

Sinaga, J. E. E., Budianto, G., Pritama, V. L., & Suhendra, S. (2023). The Lithology of Flood Prone Areas Using the Vertical Electrical Sounding (Ves) Method. *Indonesian Physical Review, 6,* 114-123. https://doi.org/10.29303/ipr.v6i1.209

Stempvoort, D. V., Ewert, L., & Wassenaar, L. (1993). Aquifer Vulnerability Index: A Gis-Compatible Method for Groundwater Vulnerability Mapping. *Canadian Water Resources Journal, 18*, 25-37. https://doi.org/10.4296/cwrj1801025

Takem, G. E., Kuitcha, D., Ako, A. A., Mafany, G. T., Takounjou-Fouepe, A., Ndjama, J. et al. (2015). Acidification of Shallow Groundwater in the Unconfined Sandy Aquifer of the City of Douala, Cameroon, Western Africa: Implications for Groundwater Quality and Use. *Environmental Earth Sciences, 74,* 6831-6846. https://doi.org/10.1007/s12665-015-4681-3

Tamfu, S., & Batupe, M. (1995). Geologic Setting, Stratigraphy and Hydrocarbon Habitat of the Douala Basin (Cameroon). *National Hydrocarbon Journal of Cameroon, 3,* 6.

Tchameni, F. E. (2020). *Mise en place d'un SIG de prévention des risques d'inondation dans le bassin versant du Tongo—Bassa à Douala (Cameroun).* Ph.D. Thesis, Université de Douala.

Udosen, N. I., Ekanem, A. M., & George, N. J. (2024). Geo-electrical Prognosis of Aquifer Protectivity, Corrosivity, and Vulnerability via Index-Based Models within a Major Coastal Milieu. *Discover Geoscience, 2,* Article No. 18. https://doi.org/10.1007/s44288-024-00020-6